Journal of Molecular Liquids 337 (2021) 116579

Contents lists available at ScienceDirect

Journal of Molecular Liquids

journal homepage: www.elsevier.com/locate/molliq

Efficient parameterization of intermolecular force fields for molecular dynamics simulations via genetic algorithms

Abdullah Bin Faheem [a], Jong-Yun Kim [b,c], Sang-Eun Bae [b,c], Kyung-Koo Lee [a,*]

[a] Department of Chemistry, Kunsan National University, Gunsan, Jeonbuk 54150, Republic of Korea
[b] Nuclear Chemistry Research Team, Korea Atomic Energy Research Institute, Daejeon 34057, Republic of Korea
[c] Radiochemistry & Nuclear Nonproliferation, University of Science & Technology, Daejeon 34113, Republic of Korea

ARTICLE INFO

Article history:
Received 6 April 2021
Revised 14 May 2021
Accepted 24 May 2021
Available online 27 May 2021

Keywords:
Genetic algorithm
Molecular dynamics simulation
Force field
Parameterization
Acetonitrile

ABSTRACT

The development of van der Waals (vdW) parameters for molecular dynamics force fields typically requires fitting the parameters to reproduce experimental physical properties, such as the density or the heat of vaporization. These fitting procedures depend on a limited number of conformations, involve expensive DFT calculations, or need hand-tuning of the resulting parameters. Such methods have little to no support for the simultaneous fitting of the parameters, are time-consuming, and neglect coupling effects since each parameter is fitted individually rather than a common set of calculations where all parameters are derived simultaneously. Hence, in this study, we present a genetic algorithm (GA) that automates this fitting process. In this manner, the GA-based optimization can fit all the vdW terms at the same time and does not require any physical intervention. Once executed, the GA will automatically determine the optimum parameter set based on the properties included in the fitness function. The GA reported herein has been successfully applied to acetonitrile, a common organic solvent, to reasonably reproduce both the thermodynamic and dynamic properties at room temperature as well as in a wide temperature range. The use of GA not only serves as a powerful optimization tool but also opens up new avenues in the development of accurate force fields that can provide valuable molecular insights.

1. Introduction

Classical molecular dynamics (CMD) is a powerful tool for studying the structure and dynamics of molecules at the atomic level. Simulations based on classical force fields permit the user to work with large systems and long simulation times. Although they cannot be used to describe electron transfer or bond formation and dissociation, they are incredibly useful in investigating the time dependence of systems containing thousands or millions of atoms. Hence, CMD has become invaluable in studying systems that include but are not limited to biomolecules [1–3], surface science [4–6], and liquid-phase calculations [7–9].

The success of the CMD calculations is determined by their ability to accurately reproduce experimental properties. However, the accuracy of CMD simulations is highly dependent upon the force field, i.e., the functional form for the potential energy, and the parameters used to define the intra- and intermolecular interactions in the system. In traditional all-atom force fields such as GROMOS [10], AMBER [11,12], OPLS [13,14], and CHARMM [15,16], the intramolecular parameters include the equilibrium bond lengths, bond and dihedral angles, along with the corresponding force constants and rotational barriers (for dihedral terms), while the intermolecular interactions are normally described by atom-centered partial charges and van der Waals (vdW) parameters. Ideally, general force fields should be *complete* and *transferable* [17]. The term *complete* implies that the general force field should have full parameter sets for most compounds, while *transferable* means that the force field should be transferable between different molecules. For example, the parameters for the methyl group in *n*-hexane, 1-hexene, or 1-hexanol should be identical. These force fields employ very similar methodologies in developing parameters, which utilize extensive experimental or quantum calculation data sets for different types of molecules. As such, general force fields are usually applicable to a large variety of systems.

For example, the intramolecular force field parameters in AMBER, OPLS, and CHARMM are normally fitted against DFT calculations at the appropriate level of theory [13,16,18]. Typically, it is preferred that the level of theory used is not computationally expensive and produces the least error. For the bond and angle parameters, the harmonic potential for the bonds and angles may

* Corresponding author.
E-mail address: kklee@kunsan.ac.kr (K.-K. Lee).

https://doi.org/10.1016/j.molliq.2021.116579
0167-7322/

be simply obtained by scanning a set of structures by varying the bond and angle values and plotting the energy profiles obtained from the different structures. The equilibrium values correspond to the bond or angle value that gives the lowest energy. The associated force constant is obtained by fitting a quadratic function around this minimum. The equilibrium bond and angle values and their force constants can also be obtained from experimental data such as infrared, microwave, or X-ray and neutron diffraction studies and are compared to values obtained from CMD calculations.

Although the dihedrals are described by a more complex function for potential energy, they are parameterized in a similar way to the bond and angle terms. A scan of energies of many possible torsion angles is conducted [13,16,18]. The obtained energies are fitted to a truncated Fourier series. Usually, the performance of the dihedral terms is evaluated by comparing the rotational scan about the dihedral of interest obtained from CMD to quantum calculations.

The nonbonded interactions consist of two main components, namely, the electrostatic and vdW forces. The electrostatic interactions are described by Coulomb's law, where the interaction energy is proportional to the partial charges of the species. In contrast, the vdW interactions are most commonly defined using the Lennard-Jones (L-J) potential function. Although different interatomic potentials for the vdW interactions have been reported, such as the Buckingham potential, the Born–Meyer–Huggins potential, the Tersoff potential, or the embedded-atom potential, the L-J potential remains the most widely used intermolecular potential in classical many-body simulations. The reason for this is mainly because of its simplicity and low computational cost; the use of a simple functional form with a fewer number of optimizable parameters makes the L-J potential easy to use and computationally inexpensive. Therefore, in commonly available force fields such as AMBER, OPLS, and CHARMM, the vdW terms are represented by the L-J potential. Because the L-J terms are tightly coupled to the electrostatic terms, different force fields adopt different approaches in parameterizing the intermolecular terms. For instance, in OPLS and CHARMM, the vdW parameters are parametrized alongside the atomic partial charges. In this case, the nonbonded parameters are optimized to reproduce ab initio interaction energies and are validated against liquid-state experimental properties, such as the heat of vaporization and density. The partial charges are often subjected to further optimization using the popular ChelpG scheme, which fits the atomic charges to the quantum mechanical electrostatic potential (ESP) surrounding a molecule [19–23]. This is in stark contrast to AMBER, where the partial charges are obtained on a case-by-case basis and are derived to reproduce the ab initio molecular ESP using the RESP approach [24]. Then, the vdW terms are parameterized separately and validated against experimental properties.

As mentioned previously, the accuracy of CMD calculations is dependent upon the empirical parameters that define the potential energy of the system. While the intramolecular parameters influence the structure of the molecule, the intermolecular parameters describe the interactions between different molecules. Therefore, the intermolecular interactions heavily influence the physical properties of the system, i.e., density, heat of vaporization, diffusion coefficients, etc. Nonbonded parameters require special attention to define accurately the physics of any system. For assigning partial charges, methods such as RESP and ChelpG are already well established. On the other hand, a universal or widely accepted method for deriving vdW parameters does not exist. After the determination of the partial charges, the vdW terms are adjusted to reproduce high level ab initio or experimental data [25].

The vdW parameters in commonly available force fields such as AMBER, OPLS, and CHARMM are typically refined to reproduce liquid-state properties such as densities and heats of vaporization [13,16,18]. Nevertheless, because parameters in general force fields are optimized purely based on condensed phase properties and at room temperatures, they may not produce valid results in the gas or solid phase or at different temperature conditions. For example, Kaminski et al. observed that the OPLS force field is unable to predict the gas-phase dimerization energies of methanethiol and ethanethiol even though their liquid-state properties were in very good agreement with the experimental results [13]. In addition, presently available general force fields are not consistent in their performance for different types of molecules. This has been investigated extensively by Wang et al., where the General AMBER Force Field (GAFF) was used to perform CMD simulations of different molecules [26,27]. As pointed out by Wang et al., while as a whole the average percentage error can be quite reasonable, the GAFF parameters perform well in some cases and poorly in others. For example, the diffusion coefficients obtained for proteins in aqueous solutions reproduced experimental data to a much better extent in comparison to organic solvents [26]. These deviations from experimental results were mainly attributed to the presence of unoptimized vdW parameters. Similar results have been reported in previous literature as well, where researchers have either tested out different parameter sets or fine-tuned a set of vdW parameters according to their needs [28–35]. As such, because the intermolecular vdW parameters heavily influence the physical properties of the system, the need for parameter sets that can reproduce experimental data is crucial.

Methods for deriving parameters during force field development employ a limited number of molecular conformations to determine force field parameters from DFT calculations. Usually, the parameters obtained from quantum mechanical calculations require further hand-tuning to match experimental physical properties [18,29]. Such methods have little to no support for the simultaneous fitting of the parameters, resulting in a large number of calculations and neglect coupling effects because each parameter is fitted individually rather than a common set of calculations where all parameters are derived simultaneously. This is particularly the case for the vdW parameters, which are tightly coupled with one another. As the hand-tuning approach involves fixing a certain parameter and adjusting the remaining parameters, the required calculations become increasingly expensive as the number of parameters increase.

For small molecules with a few parameters, hand-tuning the vdW terms might be successful. However, for large molecules, this might not be possible due to the multidimensional parameter space and the inherent coupling of those parameters. Nevertheless, this can be long and tedious even for small molecules because one has to rely on one's chemical intuition to guess which set of parameters might provide an acceptable description of the system and if needed, manually vary each parameter to search for a set that most accurately describes the physics of the system. Such a hand-tuning approach requires an intimate knowledge of the chemical structures of the molecules simulated, which might not always be possible [29].

Recently, genetic algorithms (GA), an example of a very efficient optimization algorithm, have been widely used by chemists to optimize MD force field parameters. GAs have been successfully used to optimize dihedral terms [17,18], vdW parameters [25], atomic charges [24] and polarizability [36], and reactive [37] and coarse-grain [38] force fields. GAs are a class of evolutionary algorithms that attempt to simulate the process of biological evolution through steps such as selection, mutation, and crossover. Just as in nature where organisms fight to survive, the genes that produce the best individuals survive and reproduce. The power of the GA lies in its ability to efficiently deal with multidimensional or nonlinear problems and complex and poorly understood search spaces

[24]. In GAs, first an initial set of chromosomes or the initial population is generated. In the context of GAs, the aforementioned genetic material or a chromosome can be any set of parameters that give a solution or result. The initial population is then evaluated via a scoring function, or in other words a fitness function, where a better fitness value indicates a superior performance of the parameter set. Next, in the selection operation, chromosomes with high fitness get to propagate to the next generation, and those having low fitness perish. The probabilistic selection of organisms for mating introduces additional variety into the population and prevents falling into a local minimum. New chromosomes are then generated through the crossover and mutation steps. The new genes extend the reach of the algorithm outside the pool of values from the previous generation.

While GAs have been used by previous researchers in optimizing or developing parameter sets for CMD, most studies have focused on developing intramolecular parameters. For example, Wang et al. introduced "*Parmscan*," an automatic search engine that utilized GAs to optimize the torsional parameters for the AMBER force field [17]. In the aforementioned study, the Fourier terms for dihedral parameters in the AMBER force field were developed to reproduce the relative energies of 11 different hydrocarbons obtained from quantum calculations. Similarly, the GA module "*Paramfit*," was developed to optimize the bond, angle, and torsional parameters for CMD by fitting the parameters against energy calculations at the quantum level [18]. The software module was tested by developing the dihedral parameters for alanine tetrapeptide and lipid tails. In a study by Courcot et al., the intramolecular parameters for polymolybdate and polytungstate clusters were developed by comparing the equilibrium structures from CMD to X-ray diffraction studies [39]. However, since intermolecular interactions can heavily influence the physical properties of the system, protocols for parameterizing the vdW interactions require special attention. Nevertheless, to the best of our knowledge, only a limited number of GA studies have been conducted for the development of vdW parameters. For instance, Wang et al. employed the use of GA for developing the vdW parameters for pure organic liquids, where the optimization scheme used experimental densities and ab initio interaction energies to fit the parameters [25]. However, such a methodology does not take into account the dynamic properties of the system, such as the diffusion coefficient or the viscosity. Furthermore, because the densities were estimated from intermolecular interaction energies and were verified only at certain temperatures, it is not evident whether the performance of the parameters optimized by GA is consistent at different temperatures. In another study by Chen et al. [40], the vdW parameters for metal–organic frameworks (MOFs) were optimized for predicting the CO_2 and CH_4 adsorption isotherms in MOFs. The parameters were optimized to reproduce ab initio interaction energies and the CMD-obtained adsorption isotherms were validated against experimental data. Therefore, it is apparent that GA studies on the development of intermolecular vdW parameters are scarce. As discussed previously, since the vdW parameters heavily influence the physical properties of the system, work on the development of optimization protocols for the vdW parameters requires significant attention.

Hence, in this study, we investigate the use of GAs and their application in the parameterization of the intermolecular L-J parameters for classical force fields. Using acetonitrile (ACN) as the case study in this work, we present an optimization scheme that is not only able to reproduce experimental physical properties for a wide temperature range but also the microstructural characteristics obtained from highly accurate first-principles MD (FPMD) and experimental data. In this work, the reasons for choosing ACN are twofold: (1) it is a very common organic solvent with a wide range of applications and (2) is the subject of extensive manual parameterization that can be directly compared to the GA's performance [29,35]. From the results reported herein, the use of GA proved to be incredibly efficient in finding the global minimum and thus a more practical solution to parameter optimization problems in comparison to the traditional hand-tuning approach.

2. Methodology

2.1. Force field

In this study, we employ the following all-atomic force field, which describes the intra- (U_{intra}) and intermolecular (U_{inter}) interactions as follows:

$$U_{intra} = \sum_{Bonds} K_b(b - b_0)^2 + \sum_{Angles} K_\theta(\theta - \theta_0)^2 + \sum_{Dihedrals} \frac{V_n}{2}(1 + \cos[n\varnothing - \delta]) \quad (1)$$

$$U_{inter} = \sum_{i=1}^{N-1} \sum_{j=i+1}^{N} \left\{ 4\varepsilon_{ij} \left[\left(\frac{\sigma_{ij}}{r_{ij}}\right)^{12} + \left(\frac{\sigma_{ij}}{r_{ij}}\right)^{6} \right] + \frac{q_i q_j}{r_{ij}} \right\} \quad (2)$$

where b, θ, n, and $\varnothing$ are the bond length, angle, dihedral multiplicity and dihedral angles, respectively. The b_0, θ_0, and δ values represent the equilibrium values of the bond, angle, and dihedral terms; and K_b, K_θ, and V_n are the associated force constants. The L-J parameters in Eq. (1), ε_{ij} and σ_{ij}, are obtained from the Lorentz–Berthelot mixing rules in Eq. (3). The nonbonded electrostatic interactions are described by the last term in Eq. (2), where q_i and q_j are the partial charges of atoms i and j, respectively, and r_{ij} represents the distance between those atoms.

$$\varepsilon_{ij} = \sqrt{\varepsilon_{ii}\varepsilon_{jj}}, \ \sigma_{ij} = \frac{(\sigma_{ii} + \sigma_{jj})}{2} \quad (3)$$

As this study uses GA to optimize the L-J parameters for ACN, this leads to 8 adjustable terms. These are the ε_{ii} and σ_{ii} values of 4 different atom types (see Fig. 1).

For the intramolecular terms, the equilibrium bond lengths, angles, and torsional angles for ACN were determined from DFT calculations at the MP2/aug-cc-pvtz level via Gaussian 09 [41], while the force constants were extracted from the GAFF parameter set. Subsequently, the partial charges of the molecules studied were obtained from the ESP of the optimized structures, using the RESP method available in the AMBER 12 package [42]. Previously developed general force fields have employed the use of the HF/6-31G* level of theory to obtain the ESP. However, it is well-known that this method uniformly overestimates molecular polarity. Indeed, the HF/6-31G* theory level yields dipole moments that are approximately 10% larger than those observed in the gas

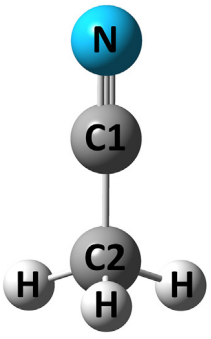

Fig. 1. Structure of ACN with atomic labels. Colors: nitrogen, blue; carbon, gray; hydrogen, white.

Table 1
Optimized L-J parameters obtained from GA. Refer to Fig. 1 for atom-type definitions.

Atom-type	σ (Å)	ε (kJ mol^{-1})
N	3.1106	0.5600
C1	3.5422	0.5312
C2	3.3199	0.4530
H	2.4574	0.0188

phase [12,43]. This difference is exploited in condensed phase simulations because it takes into account the implicit polarization of the molecule.

Alternatively, polarization effects can be included in the vdW parameters as well. For example, Nikitin et al. used DFT calculations at the MP2 level of theory to reproduce experimental dipole moments for ACN and then optimized the L-J parameters against experimental physical properties [44]. Similarly, since the GA reported in this study takes into account the polarization effects with the optimized L-J terms, the ESP was calculated using the B3LYP/6-311G++(d,p) level of theory. Such a method was chosen because the calculated dipole moment (4.08 D) was much closer to the experimental value (3.92 D) than that obtained from HF/6-311G+(d) (4.24 D) or MP2/6-311G++(d,p) (4.30 D) [45,46].

2.2. Van der Waals parametrization

The classical representation of genes in GAs is in the form of a string of bits, i.e., 0s and 1s. Such types of GAs are also referred to as binary-coded GAs. The bit strings in such GAs undergo crossover and mutation steps to produce the offspring and are converted to real values to express the genes. In this manner, binary-coded GAs intuitively mimic biological evolution. For the case of force field optimization, the bit strings are converted to real values, which in turn are used as parameters to run CMD simulations. The trajectories obtained with the parameters are then evaluated using the GA algorithm. Binary-coded GAs have been previously used in the development of force fields. In a study by Angibaud et al., binary-coded GAs were used to optimize the reactive force field for silicon [47]. However, for bit strings, changing a single bit can result in a large change in its real value counterpart. Thus, binary-coded GAs are suitable for exploring a wide parameter space because of the characteristics of the binary representation of genes. However, because CMD simulations are sensitive to the values of the force field parameters, a large change in the parameters from one generation to the next can introduce unrealistic solutions into the population, making binary-coded GAs unattractive for force field optimization.

An alternative to binary-coded GAs is using real values directly to create the offspring, also called real-coded GAs. Real-coded GAs hold a particular advantage over the binary representation of genes, where it is possible to limit the range within which the offspring population is obtained. In other words, the offspring do not contain genes that are substantially different from those of their parents. For the case of force field optimization, the starting parameters for GA are already predefined from quantum calculations or general force fields. Since parameters for CMD contain the physical properties of the target molecules, it is crucial to search the parameter space that is physically meaningful and large changes between the parameters of subsequent generations are not necessary and might give unrealistic parameters. Therefore, in this study, we employ the use of real-coded GAs, where the real values were used directly to create offspring.

The flow chart in Fig. 2 displays an overview of the main steps performed by the GA used in this work. In the beginning, an initial population is created. Then, the parameters in the initial population are used to run CMD calculations, after which, the properties obtained from the CMD simulations are used to calculate the fitness values of the population. Following the CMD simulation and the determination of the fitness values, the offspring are produced after a sequence of steps, namely, selection, crossover, and mutation. In the selection step, a mating pool is generated, which is used to create the next generation. The GA operators, crossover and mutation, are then applied to the individuals in the mating pool to obtain the offspring. The GA used in this study employs elitism, where the best parents are introduced into the offspring population without any changes (described later). These steps are repeated until the desired termination criteria is reached.

Before starting the GA-based optimization, the appropriate population size should be determined to minimize the number of evaluations. The number of evaluations is obtained by multiplying the total number of generations taken for the GA's convergence by the population size. In general, the optimum population size can vary significantly and is highly dependent on the optimization problem. In an analysis of previous studies where GAs were used to optimize parameters for CMD force fields, the population sizes used were observed to vary from 12 to 128 [18,24,47–49]. For example, Leonarski et al. reported that increasing the population size from 128 to 8192 did not result in better fitness values [38]. In another study by Marques et al., increasing the population size from 12 to 60 while keeping the number of evaluations the same, did not improve the final results [48]. This implies that if the population size is greater than a certain value, better parameters and a decrease in the total number of evaluations cannot be achieved. Hence, we have opted to use a population size of 12, the smallest reported population size for force field optimization. From the results described herein, it is evident that such a population size is sufficient for converging to an optimum solution in a reasonable number of generations.

To generate the initial population, we used the parameters from GAFF. At the beginning of the optimization, an initial population is generated by randomly selecting parameters within 10% variance of the GAFF parameters. The parameters obtained at each generation are used to run CMD simulations. From these, the physical properties, i.e., the densities and diffusion coefficients, are determined and used to calculate the fitness value using Eq. (4). Individuals with a low fitness function value encode better solutions (are more fit) and are better able to reproduce experimental densities and diffusion coefficients. The density and diffusion coefficient were used in the fitness function to replicate the experimental equilibrium and dynamic characteristics of the system.

$$\text{Fitness} = 100 \times \left(\frac{\left|\rho^{calc} - \rho^{exp}\right|}{\rho^{exp}} + \frac{\left|D^{calc} - D^{exp}\right|}{D^{exp}} \right) \tag{4}$$

In Eq. (4), the ρ^{calc} and ρ^{exp} represent the calculated and experimental densities, respectively, while D^{calc} and D^{exp} are the calculated and experimental diffusion coefficients, respectively. A point to be noted is the exclusion of any adjustable weighting factors in Eq. (4). Normally, the fitness function includes more than one term against which the CMD parameters are fitted and usually includes weighting factors [25,38,50]. By adjusting the weighting factors, one can consider the contribution of one term to be more than the other terms during parameter optimization. However, as there is no clear link between the MD parameters and a given physical property, the use of such a method might produce a force field that is biased only toward a particular physical property, which is undesirable. Hence, we employ a more general-purpose fitness function that does not include weighting factors. In Eq. (4), the absolute difference (for example, $|D_{calc} - D_{exp}|$) is divided by the experimental value, which normalizes the values of each term in Eq. (4) and allows equal contribution from all terms. In this work, the density and diffusion

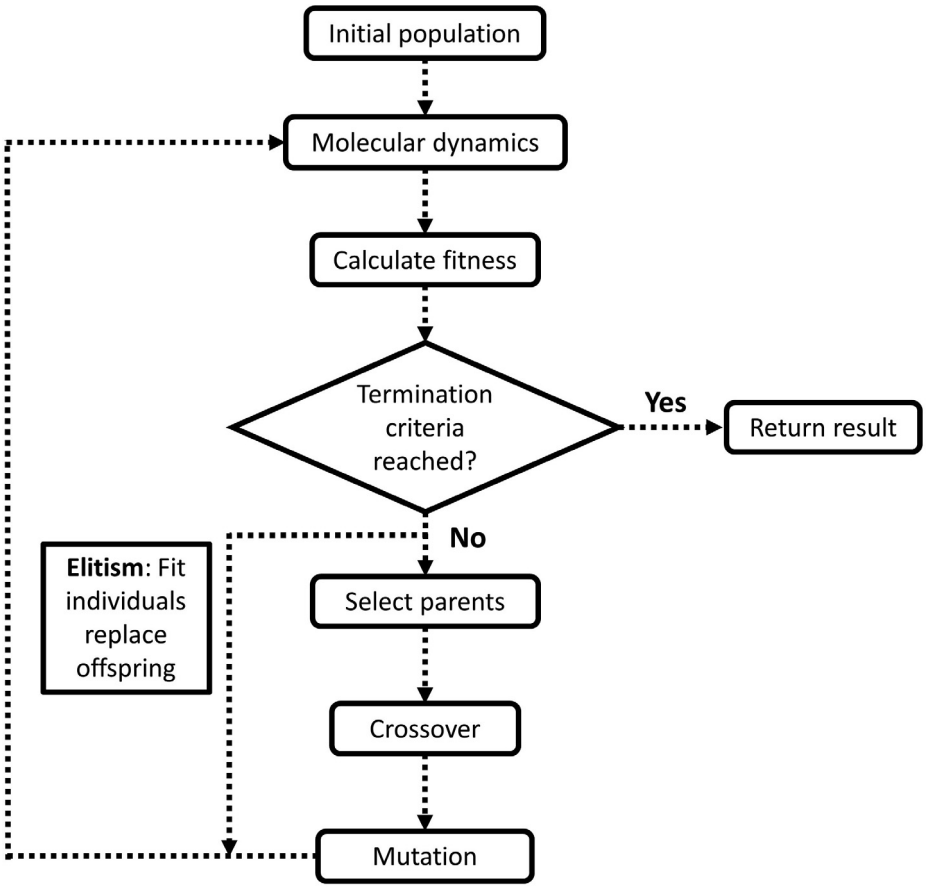

Fig. 2. Flowchart of the genetic algorithm used herein.

coefficient of ACN at 298 K, i.e., 0.7766 g cm^{-3} and 4.34 × 10^{-5} cm^2 s^{-1}, respectively, were used as the experimental values in the fitness function [29,35,51,52].

The GA used herein adopts elitism, where the fittest individuals are guaranteed a place in the next generation. Individuals with high fitness values can be lost if they are not selected to reproduce or if crossover or mutation operators change them. Elitism can significantly improve the GAs performance since it can be used to eliminate the chance of any undesired loss of information during the crossover or mutation stages [53–55]. Therefore, based on the fitness function (Eq. (4)), the parents are ranked and the top two fittest parents are propagated into the offspring population without alterations.

The selection operator selects suitable candidates for the mating pool from the parent generation. We employed the use of the tournament-type selection because this selection method was observed to work well with the crossover operator (discussed later) used in this study [48]. The tournament-type selection step consists of picking two random individuals from the parent population and comparing their fitness values. The individual with a higher fitness value is selected and added to the mating pool. This process is repeated until the desired population size is reached (12 in this case). A schematic of the tournament-type selection is illustrated in Fig. 3(a).

For the crossover operator, care should be adopted, as it is the main part of the GA algorithm that is mainly responsible for exploring the parameter search space. An example of a common crossover method is shown in Fig. 3(b), termed the one-point crossover. This crossover operator is considered to be among the class of discrete recombination operators. In the one-point crossover, after selecting a random cut point along the sequence of the two parents, the children are obtained by swapping the parameters among the two parents [48]. However, for real-coded GAs, discrete recombination operators cannot introduce new values into the next generation; they just rearrange existing ones. This results in a poor sampling of the search space and may require large population sizes (as discussed previously). An alternative to discrete recombination operators is the use of arithmetic crossover operators, where the children are produced from the weighted average of the parents. Such crossover methods can introduce new values into the offspring population and possess a greater search power in comparison to the discrete recombination operators. The simulated binary crossover (SBX) is a well-known example of an arithmetic crossover operator and has achieved good results in several problems of varying difficulty and dimensionality [48,54]. An illustration of the SBX crossover is presented in Fig. 3 (c). In the SBX crossover, the offspring (Child 1 and Child 2) are obtained from the parents (Parent 1 and Parent 2) in the following manner [48]:

(1) select a random value, μ, that is between 0 and 1
(2) calculate β, where.

$$\beta = (2\mu)^{\frac{1}{n+1}}, \text{ if } \mu \leq 0.5 \quad (5)$$

$$\beta = \left(\frac{1}{2(1 - \mu)}\right)^{\frac{1}{n+1}}, \text{ if } > 0.5 \quad (6)$$

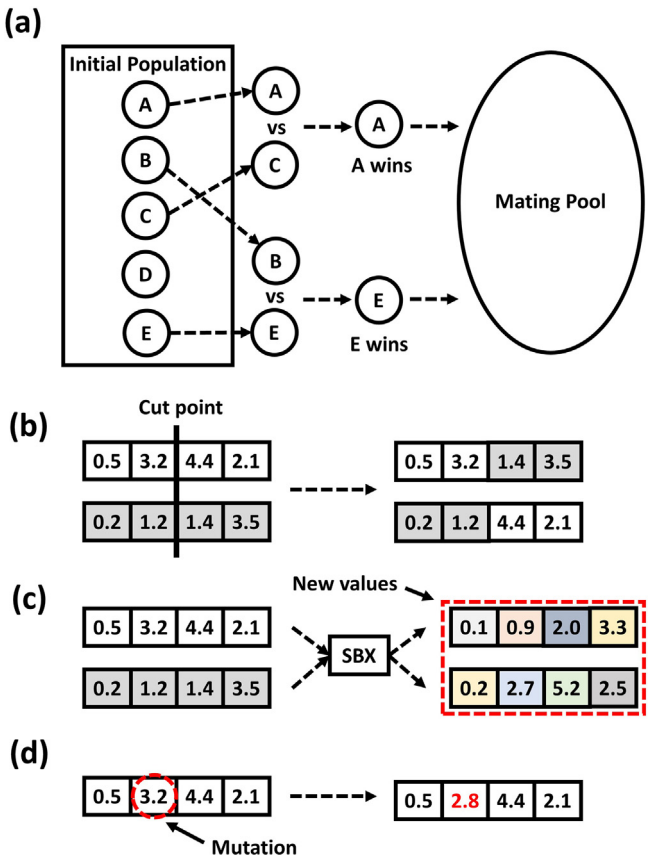

Fig. 3. Schematic illustration of the (a) tournament-type selection, (b) one-point crossover, (c) SBX crossover, and (c) mutation operator. The letters, i.e., "A," "B," or "C," represent the individuals in the parent population.

(3) obtain children

$$\text{Child 1} = 0.5[\{(1+\beta)\times \text{Parent 1}\} - \{(1-\beta)\times \text{Parent 2}\}] \quad (7)$$

$$\text{Child 2} = 0.5[\{(1+\beta)\times \text{Parent 1}\} - \{(1-\beta)\times \text{Parent 2}\}] \quad (8)$$

where n is a nonnegative real number. Large values of n create offspring that are close to their parents, while a small n allows distant values to be selected for the children [48]. In this manner, selecting a large n value produces offspring that lie within a reasonable range of possible solutions. A value of n = 50 was selected for this study and a crossover probability of 100% was employed, implying that all the children were created through the SBX crossover method.

In GAs, the mutation operator causes a random jump from the original value (Z_{org}) in a solution set to a mutated one (Z_m). This is in stark contrast to the crossover operator, where two parents are used to generate the offspring, as seen in Eqs. (7) and (8). However, for developing CMD force fields, if the difference between Z_m and Z_{org} is large, the offspring population may contain unreasonable values. Therefore, the mutation operator used herein changes the value (Z_{org}) of a random parameter in the offspring population by ±10%. The probability of an individual to undergo mutation was set to 5%.

$$Z_m = Z_{org} + [Z_{org}\times N(-0.1, 0.1)] \quad (9)$$

where $N(-0.1, 0.1)$ represents a random value between −0.1 and 0.1.

It is important to note that the choice made for the crossover and mutation probabilities may be further optimized by conducting a rigorous evaluation of all possible combinations. However, the results in Section 3 indicate a favorable GA performance and thus the used methods are sufficient.

2.3. Classical molecular dynamics

The starting configuration for performing CMD simulations with GA-derived parameters at each generation was generated using the GAFF parameters. Usually, at the beginning of the CMD, simulations in the *NPT* ensemble are conducted to equilibrate the simulation box. Such calculations may require simulation times in the range of several tens of nanoseconds. However, since the starting structure used herein is pre-equilibrated by GAFF parameters, computational overheads from these long simulations in the *NPT* ensemble are eliminated, thus substantially reducing the overall time taken for each GA generation.

To obtain the starting pre-equilibrated structure, first, an initial configuration was generated via Packmol [49]. The systems simulated contained 512 ACN molecules that were placed in a cubic box. Then, the simulation box was heated from 0 to 800 K for 1 ns. This was followed by a 1 ns cooling step from 800 to 298 K. Both the heating and cooling steps were performed in the *NVT* ensemble. After which, a 2 ns equilibration run was performed in the *NPT* ensemble. In order to obtain the physical properties from CMD to evaluate the fitness values of each GA generation, the pre-equilibrated box was subjected to a 1 ns *NPT* simulation to equilibrate the box with the L-J parameters from GA. This was then followed by a 1 ns production run at *NPT* to calculate the required physical properties. To examine the effect of the simulation time on the calculated densities and diffusion coefficients of pure ACN, 1 and 20 ns MD simulations (production run) were used to calculate the physical properties. It was observed that increasing the time of the production run from 1 to 20 ns lead to no statistically relevant changes in the values of the calculated densities and diffusion coefficients

All CMD simulations were performed with the LAMMPS [56] package at 298 K (unless mentioned otherwise) and 1 atm under periodic boundary conditions. The temperature and pressure were controlled by the Nosé–Hoover thermostat and barostat with relaxation times of 0.2 and 1.0 ps, respectively [35,57,58]. Equations of motion were integrated with a time step of 1 fs. The Particle–Particle Particle–Mesh algorithm was employed for long-range coulombic interactions and a cutoff of 12.0 Å was used for non-bonded interactions. The atomic coordinates were saved every 0.1 ps for analysis.

2.4. First-principles molecular dynamics

FPMD calculations were conducted using the hybrid Gaussian and Plane Wave density functional implemented in the CP2K/Quickstep program [59]. The valence electrons were described by the molecularly optimized double-ζ basis set (MOLOPT-DZVP-SR-GTH) and the Perdew–Burke–Ernzerhof functional, whereas the core electrons were treated with the Goedecker–Teter–Hutter (GTH) pseudopotentials. A total of two parallel FPMD runs were conducted. Initial configurations for the FPMD simulations were taken from random CMD snapshots using the GAFF parameters. A simulation box consisting of 60 ACN molecules was used for all FPMD simulations.

All FPMD simulations were run using the *NPT* ensemble at 298 K and 1 atm under periodic boundary conditions. The temperature and pressure were controlled via the Nosé–Hoover thermostat and barostat with time constants of 0.2 and 1 ps, respectively. The cutoff of the auxiliary plane wave was set to 500 Ry. Grimme's DFT-D3 model was also used to take into account vdW interactions [60]. A total of 100 ps of FPMD trajectory was obtained for each FPMD run, where a time step of 0.5 fs was employed and the coor-

dinates were saved every 0.01 ps. Because the energy (energy vs time) exhibited changes in the first 10 ps, the trajectory during the first 10 ps was discarded and the remaining trajectory was used for further analysis.

2.5. Physical property calculations

2.5.1. Density

The average bulk density (ρ) can be calculated from the average volume of the simulation box, $\langle V \rangle$, using Eq. (10) [25,27], where N_{res} is the number of molecules in the simulation box, M is the molar mass of ACN, and N_A is the Avogadro constant.

$$\rho = \frac{N_{res} M}{N_A \langle V \rangle} \tag{10}$$

2.5.2. Diffusion coefficient

The translational motion of a molecular species can be described by calculating the mean square displacement (MSD). This manner of analysis provides insights into the rate at which molecules move. The diffusion coefficient (D) can be obtained from the MSD via the following Einstein relation [26,29]:

$$D = \frac{1}{6} \lim_{t \to \infty} \frac{\mathrm{d}}{\mathrm{d}t} \mathrm{MSD} \tag{11}$$

$$\mathrm{MSD} = \langle (x - x_0)^2 \rangle = \frac{1}{N} \sum_{n=1}^{N} (x_n(t) - x_n(0))^2 \tag{12}$$

where $x_n(0)$ is the initial position of the molecule; $x_n(t)$ is the position of the molecule at a time t, and N is the total number of molecules.

2.5.3. Heat of vaporization

The heat of vaporization (H_{vap}) was determined using the same approach as that of Wang et al. [25], and is illustrated as follows:

$$H_{vap}(\mathrm{T}) = E_{gas}^{potential}(\mathrm{T}) - E_{liquid}^{potential}(\mathrm{T}) + RT + C \tag{13}$$

$$E_{gas}^{potential}(\mathrm{T}) = E_{gas}^{minimized}(\mathrm{T}) + \frac{1}{2} RT(3N_{atom} - 6 - N_{cons}) \tag{14}$$

where $E_{gas}^{potential}$ and $E_{liquid}^{potential}$ are the potential energies calculated in the gas and liquid phases, respectively; $E_{liquid}^{potential}$ can be directly calculated from liquid-phase MD simulations and $E_{gas}^{potential}$ can be estimated via Eq. (14); $E_{gas}^{minimized}$ is the energy after energy minimization in the gas phase; and N_{atom} and N_{cons} are the number of molecules in the simulation box and the number of constrained degrees of freedom, respectively. The correction term C in Eq. (13) accounts for the difference between the vibration energies calculated quantum mechanically and classically, as well as the polarization and nonideal gas effects. However, since in most cases C is very small, it can be neglected and was not used in this work [25,27].

2.5.4. Shear viscosity

The shear viscosity (η) can be determined from the following Green–Kubo expression where η is obtained from the autocorrelation function of the off-diagonal elements of the pressure tensor [61–63]:

$$\eta = \frac{V}{k_B \mathrm{T}} \int_0^{\infty} P_{\alpha\beta}(t) P_{\alpha\beta}(0) \mathrm{d}t \tag{15}$$

where V is the volume of the simulation box, k_B is the Boltzmann constant, and T is the absolute temperature. $P_{\alpha\beta}(t)$ is the $\alpha\beta$ component of the pressure tensor ($\alpha\beta = xy, xz, yz$; as $\alpha \neq \beta$) at time t and is calculated via the following equation [63]:

$$P_{\alpha\beta} = \frac{1}{V} \left(\sum_{i=1}^{N} \frac{p_{i\alpha}(t) p_{i\beta}(t)}{m_i} + \sum_{i<j}^{N} r_{ij\alpha}(t) f_{ij\beta}(t) \right) \tag{16}$$

$p_i(t)$ is the center of mass momentum of molecule i with mass m_i, $r_{ij} = r_i - r_j$ is the intermolecular distance, and f_{ij} is the force on molecule i by molecule j, and the summation is over all N molecules. The viscosity was calculated using an average of the P_{xy}, P_{xz}, and P_{yz} values. To obtain statistically reliable viscosity values, additional 3 ns simulations in the NVT ensemble were carried out.

3. Results and discussion

To verify the ability of the GA algorithm in optimizing the vdW parameters, the GA procedure described herein was used to develop the L-J parameters of ACN. There are two major reasons for selecting ACN to test the performance of the GA. First, ACN is a common organic solvent with a wide range of applications, and second, it has been the subject of extensive manual parameterization which can be directly compared to the GA's performance [29,35].

In this section, we present the efficiency of our GA in parameterizing the L-J terms and then discuss the performance of the optimized L-J parameters in calculating the physical and microstructural properties. To best our knowledge, this is the first study where GA has been used to derive parameters for ACN that are able to not only reproduce experimental physical properties for a wide temperature range but also structural characteristics from highly accurate FPMD and neutron scattering data.

3.1. GA force field parameterization

As discussed in Section 2, the experimental density and diffusion coefficient were used to fit the L-J parameters for ACN. Fig. 4 illustrates the evolution of the fitness, density (ρ), and diffusion coefficient (D) of the individual that has the best fitness value in the generation. Initially, the starting parameters are generated by randomly selecting parameters within 10% of the GAFF parameters and give densities and diffusion coefficients that are far away from the experimental values. This is indicated by the fitness value of the fittest individual in Fig. 4(a), which is 27.6 at the beginning. However, as the GA progresses, the fitness value decreases and eventually converges to a value of 0.42 at generation 28. Because the fitness value does not change for 20 or so generations, it can be said the L-J parameters have reached their optimum values and the GA has converged. The ρ and D values of the fittest individual at each generation in Fig. 4(b) and (c) exhibit similar behavior. In the beginning, the ρ and D deviate by approximately 13.4% and 14.2% from their experimental values (dashed horizontal lines), but as the GA progresses iteratively, they approach values almost similar to the experimental measurements. The L-J parameters obtained from the GA optimization are listed in Table 1.

To determine quantitatively the reliability of the L-J parameters obtained by GA, the physical properties (ρ, D, H_{vap}, and η) obtained using the GA-derived parameters are compared with the previously developed force fields using the mean absolute percentage error (MAPE) as follows:

$$\mathrm{MAPE} = \frac{1}{N} \sum_{i=1}^{N} \left| \frac{A_i - F_i}{A_i} \right| \times 100 \tag{17}$$

where A_i and F_i are the experimental and calculated properties, respectively, and N is the total number of properties (4 in this case).

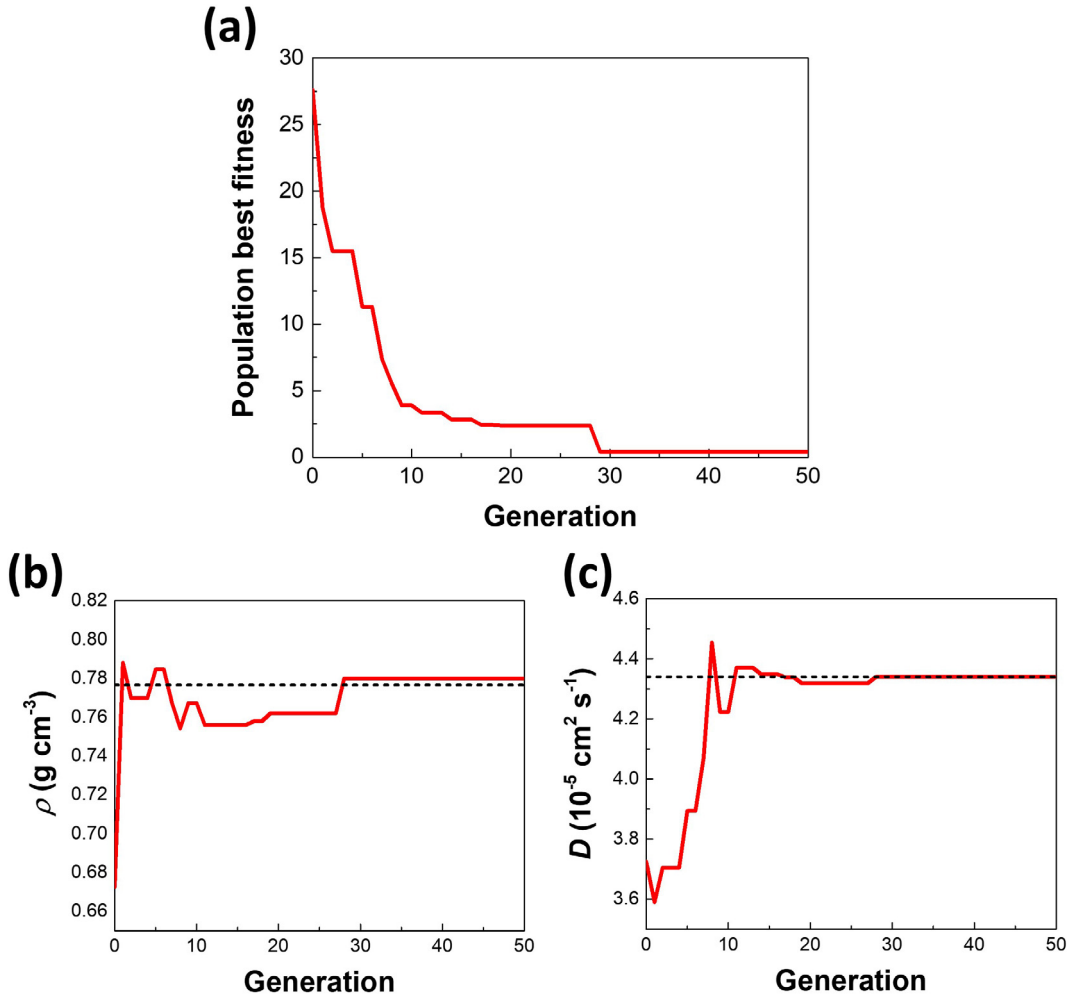

Fig. 4. (a) Fitness value, (b) density (ρ), and (c) diffusion coefficient (D) of the fittest individual in each generation. Experimental values are indicated by the dashed lines.

Table 2
Comparison between the physical properties and mean absolute percentage error (MAPE) of the force field obtained from GA optimization and the models developed in previous work (at 298 K).

Model	ρ (g cm^{-3})	D (10^{-5} cm^2 s^{-1})	H_{vap} (kJ mol^{-1})	η (mPa s)	MAPE (%)
Experiment [29]	0.7766	4.34	32.94	0.3410	–
Grabuleda et al. [64]	0.7112	4.09	30.63	0.2805	9.73
Vanommeslaeghe et al. [65]	0.7860	3.08	34.39	0.4631	17.62
Koveraga et al. [29]	0.7639	4.35	30.67	0.3188	3.81
Orhan et al. [66]	0.7555	4.75	29.79	0.2807	9.84
Kowsari et al. [35]	0.7758	3.82	32.26	0.3356	3.93
From GA	0.7799	4.34	31.13	0.3180	3.16

From Table 2, it can be observed that the GA-derived model provides the best overall results with the lowest MAPE. Therefore, the GA-optimized L-J terms can reproduce the experimental properties to a better extent overall in comparison to previously reported force fields. The performance of the GA force field is similar to the results reported by Koveraga et al. [29] and Kowsari et al. [35], where the L-J terms of ACN were parameterized by manually changing the parameters to match the experimental physical properties. A point to note is that the heat of vaporization and viscosity, which were not used in the fitness function for GA optimization, is slightly underestimated. However, the GA-derived parameters can reasonably estimate the experimental results. The comparison in Table 2 shows the ability of the GA reported herein to optimize the vdW parameters.

To test the reproducibility of the GA, additional GA optimizations were also conducted, and the statistics are presented in the supporting information. We found that, in general, there is no statistically significant difference in achieving convergence with different initial parameters. This can be seen in Table S1, where the standard deviation for the physical properties among all the GA runs was less than 0.5% of the average. This indicates the reasonable reproducibility of the physical properties by different GA runs. However, because of the random generation of the initial parameters, each different GA run might converge to a slightly different

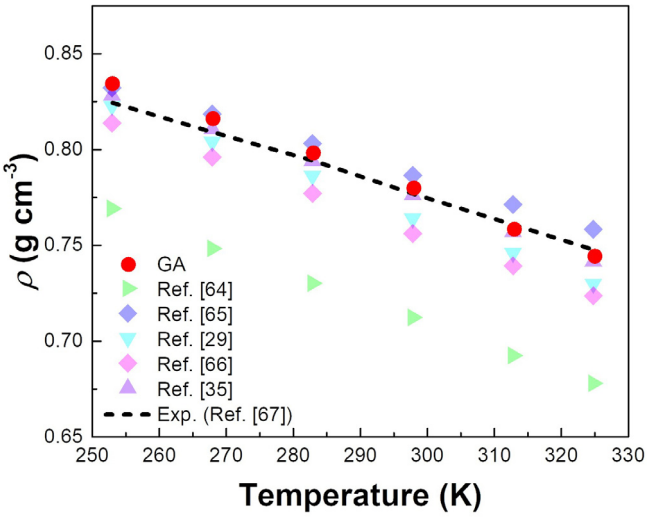

Fig. 5. Density of pure ACN at different temperatures calculated with the GA force field (red circles) and the different force fields developed by Grabuleda et al. [64] (green triangles), Vanommeslaeghe et al. [65] (blue diamonds), Koveraga et al. [29] (cyan triangles), Orhan et al. [66] (magenta diamonds), and Kowsari et al. [35] (purple triangles), in comparison with experimental measurements (solid dashed line) [67].

fitness value (Table S1). As such, several GA optimizations were performed and the parameters that gave the best fitness values among the different runs were reported.

3.2. Molecular property calculations

3.2.1. Temperature dependence of density, diffusion coefficient, and viscosity

Fig. 5 compares the temperature dependence of the density of the GA force field with previously reported force fields and experimental data from the results by Hurle et al. [67]. In general, all the force fields follow experimental trends, with the density of ACN showing a decreasing trend at increasing temperatures. However, the performances of the different force fields vary significantly. For example, while the force field by Grabuleda et al. [64] follows the experimental trends, the density is 7–10% lower than experimental results. Since this is a version of the GAFF force field for ACN, this error is most likely due to the unoptimized L-J parameters. The underestimated densities by GAFF highlight the disadvantages of using general force fields discussed in Section 1. Therefore, the development of force optimization methodologies is crucial for MD studies. In comparison with GAFF, the CHARMM force field (Vanommeslaeghe et al. [65]) gives densities that are much closer to the experimental results in comparison with GAFF. However, it does not give reasonable diffusion coefficients (which will be discussed in the following sections). From Fig. 5, the GA force field and the parameters developed by Kowsari et al. [35] exhibit the best performance at different temperatures, whereas the force fields reported by Koveraga et al. [29] and Orhan et al. [66] underestimate the densities higher temperatures. In conclusion, the calculated densities with the GA parameters well reproduce the experimental results; both the magnitudes and the overall trend for the temperature range.

The diffusion coefficients and viscosity are key physical properties because they represent the dynamics of the system. Such properties are useful in studying the motions of molecules with respect to one another and shed light on the transport mechanisms that govern the system. Therefore, to evaluate the performance of the GA force field in determining the dynamic properties of the system, diffusion coefficients and viscosities were calculated at different temperatures using the GA-derived parameters and compared with previously developed force fields and experimental results (Fig. 6). The experimental diffusion coefficients and viscosities were obtained from Hurle et al. [67] and Dymond et al. [68], respectively.

From Fig. 6(a), although all of the investigated force fields reproduce approximately similar experimental trends, differences in the performances of the different force fields are apparent. As mentioned previously, while the CHARMM force field is able to estimate the experimental densities adequately, it significantly underestimates the diffusion coefficients (by more than 25%). Similarly, previously developed force fields either reasonably reproduce densities or the diffusion coefficients. This means that none of the previously reported force fields can predict both the densities and the diffusion coefficients simultaneously. In comparison, the GA-derived parameters can reasonably reproduce both the experimental densities and diffusion coefficients. In addition to the experimental trends, because the diffusion coefficients signify the translational dynamics of the molecules, the diffusion coefficients at different temperatures can be used to calculate the activation energy needed for ACN to leave its local coordination environment. The activation energy was calculated from the Arrhe-

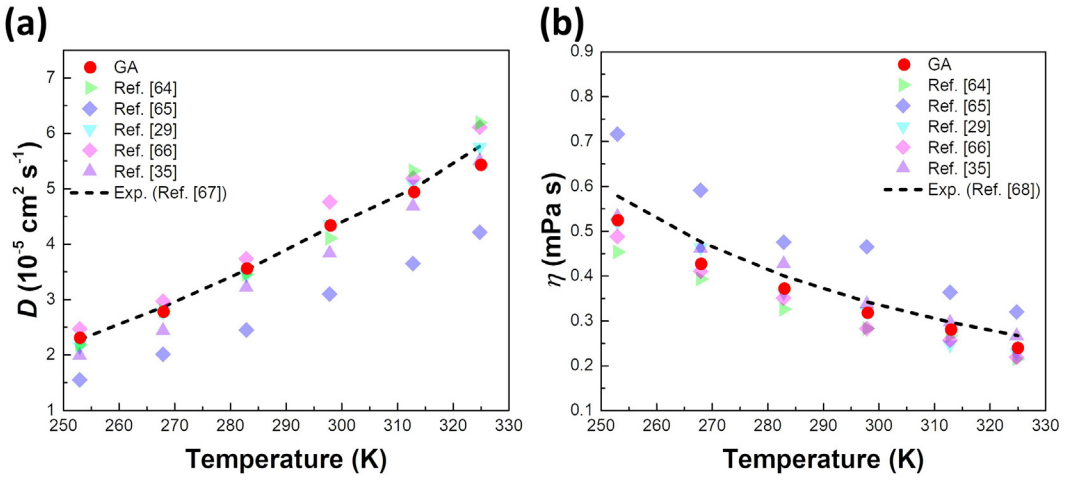

Fig. 6. (a) Diffusion coefficient and (b) viscosity of pure ACN at different temperatures obtained from the GA force field, previously developed models, and experimental data. The colors and symbols are the same as in Fig. 5.

nius plots of Fig. 6(a) and is listed in Table S2. As seen in Table S2, the GA-derived force field produces an activation energy that is closest to the experimental measurements. This shows the efficacy of the GA-derived force field in being able to provide accurate insights into the transport mechanisms affecting ACN molecules.

Further validation of the dynamic properties using the calculated and experimental viscosities is shown in Fig. 6(b). It can be observed that even though the calculated viscosities follow similar trends as the experimental values, the studied force fields are unable to accurately reproduce experimental values. Almost all the force fields in Fig. 6(b) underestimate the viscosities, while the CHARMM force field overestimates the experimental viscosities. In general, as the degree of intermolecular interactions increases, the viscosity of the system rises, and vice versa. At higher viscosities, the molecules interact more strongly with one another and move more slowly, resulting in a lower diffusion coefficient. Therefore, because the diffusion coefficient is inversely proportional to the viscosity, this explains why the diffusion coefficient with the CHARMM force field is lower than for the other force fields (Fig. 6(a)). However, even though the viscosities obtained from the GA-derived force field underestimate the experimental results, this difference is comparable to previously reported force fields. Thus, it can be stated that the model proposed in this work gives a better overall performance in predicting physical properties than previously reported force fields, especially those by Koverga et al. [29] and Kowsari et al. [35], where the L-J parameters were derived manually. This is further elaborated on in the following sections. In conclusion, the ability of the GA-derived parameters in predicting macroscopic experimental properties indicates the usefulness of the GA-based optimization reported herein.

To quantitatively compare the performances of the previously reported force fields and the GA-derived parameters reported in this study, we employ the use of 2 metrics: the absolute error (AE) and the relative error (RE) (see supporting information). The values for AE and RE are summed over the temperature range shown in Figs. 5 and 6 and are listed in Table S3. Among the investigated force fields, although certain physical properties are better predicted by other force fields and give smaller errors, our GA-derived parameters exhibit the best overall performance with small AE and RE values. In general, when using the GA force field, it is possible to reasonably reproduce both the thermodynamic and dynamic properties at room temperature as well as in a wide temperature range (Figs. 5 and 6). This signifies the efficacy of the GA methodology described in this study, which eliminates the need for manually varying the L-J parameters to reproduce the experimental measurements.

3.2.2. Radial distribution functions

The GA-derived parameters are further evaluated by analysis of the microstructures present in the system. The most obvious way to study the local organization of any system is the analysis of the radial distribution functions (RDFs). Although the RDFs between various atom pairs have been investigated in previous work [29,35], these studies offer no concrete verifications of the shape and magnitudes of the RDFs illustrated and are only compared with other CMD models for ACN. Hence, to verify the validity of our model's ability to accurately represent the microstructural characteristics of ACN, we compare the CMD results with highly accurate FPMD and neutron scattering data [69]. Fig. 7 illustrates RDFs calculated from both CMD and FPMD, while Figs. S1 and S2 are the experimental neutron scattering results obtained from the work by Humphreys et al. [69].

From Fig. 7, it is evident that the CMD can reproduce the FPMD and experimental results to quite a reasonable extent. The N–N RDF in Fig. 7(a) obtained from CMD shows a double peak at approximately 4.25 and 5.45 Å. This directly coincides with the FPMD results where the first and second peaks are located at about

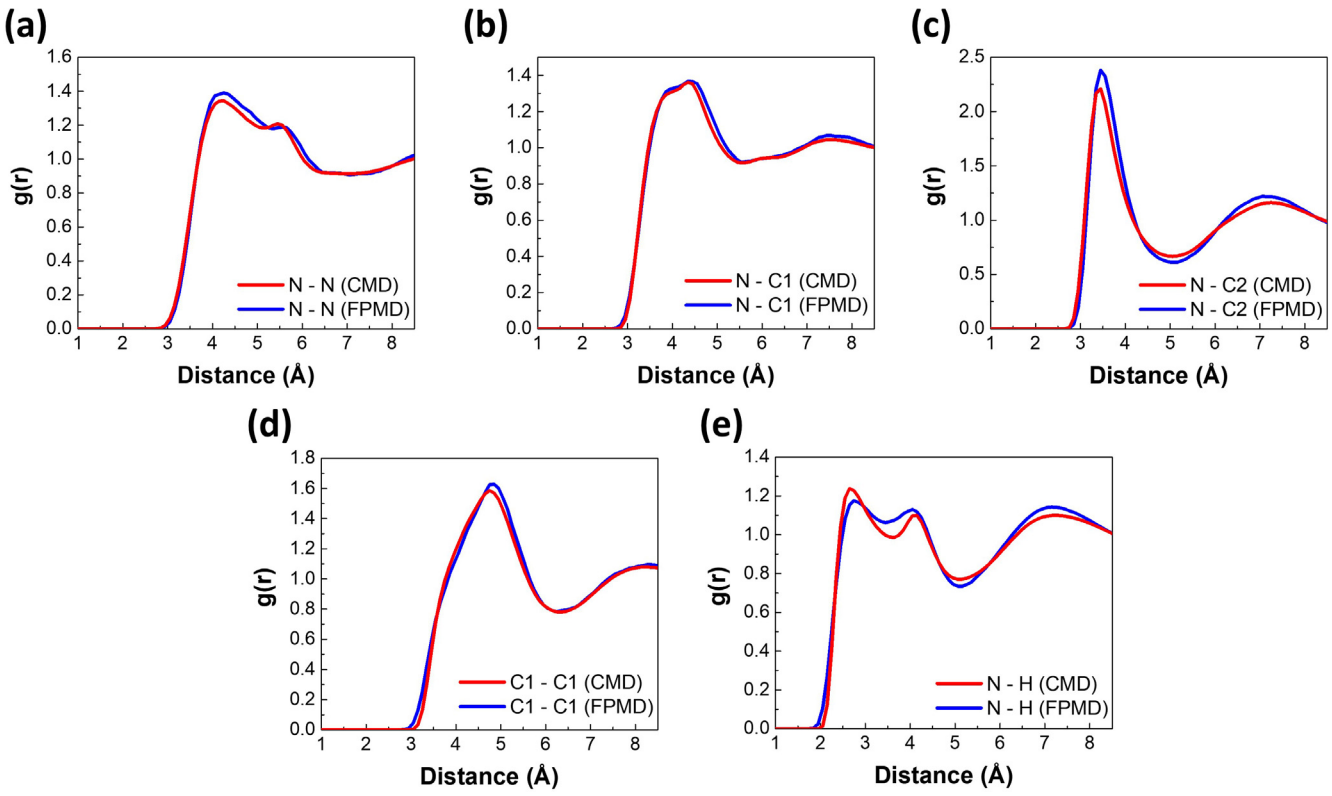

Fig. 7. Site–site RDFs (at 298 K) from CMD (GA-derived parameters) and FPMD for the (a) N–N, (b) N–C1, (c) N–C2, (d) C1–C1, and (e) N–H atom pairs in ACN.

4.25 and 5.55 Å, respectively. These results are similar to experimental measurements seen in Fig. S1 as well, where the first N–N peak is located at 4.1 Å. However, a point to be noted is the absence of a second N–N peak in Fig. S1. As the second peak in Fig. 7(a) is quite small, it is likely that it is not observed in the experimental diffraction data. The broad C1–C1 peak in Fig. 7(b) at 4.35 Å (for CMD) overlaps with the first N–N peak, similar to what can be seen from the FPMD (at 4.45 Å) and experimental measurements (at 4.5 Å) (Fig. S2). RDFs obtained from CMD indicate that the probability of finding a methyl group near the nitrogen is higher in comparison to its counterparts. This is apparent in Fig. 7(c), where the peak for the N–C2 RDF is the highest among all the RDFs in Fig. 7 for CMD (at 3.45 Å), FPMD (at 3.45 Å), and Fig. S1 (at approximately 3.4 Å). This has been linked to the strong interactions between the positively charged hydrogen and the negatively charged nitrogen [35]. Previous MD studies on ACN have also pointed towards the presence of weak hydrogen bonds between the nitrogen and the methyl hydrogen atoms [29,35]. In previous studies, it has been reported that the location of the first N–H peak was reported shortest among all pair interactions in ACN molecules. This is true for the MD simulations conducted in this study as well where the first peak for the N–H RDF in Fig. 7(e) is at 2.65 Å and 2.75 Å for CMD and FPMD, respectively. The N–H RDF also indicates the presence of a secondary peak in both the CMD and FPMD, at 4.05 Å. The calculated N–H RDF peaks are similar to the neutron scattering measurements, where the first and second N–H peaks are located at approximately 2.7 and 3.8 Å, respectively (Fig. S1). Thus, it is clear from the results herein that our GA force field can reasonably predict the intermolecular interactions in ACN, as confirmed by RDFs obtained by FPMD and experimental neutron scattering data.

The use of highly accurate FPMD simulations and experimental measurements to validate the intermolecular structures in ACN has previously not been investigated and as such we believe the methodology adopted in this study provides a more reliable way to verify the structural properties from CMD simulations. From the RDFs in Fig. 7, it is apparent that the force field optimized using GA is not only able to reproduce the physical properties but also the microstructures present in liquid ACN.

3.2.3. Reorientational dynamics

The diffusion coefficients and viscosities investigated in previous sections are properties that measure the translational dynamics of the system. However, the rotational or reorientational dynamics of a molecule can also be considered to be important. Similar to the translational motion, the rotation of the molecule is directly affected by its local environment. Therefore, the rotational or reorientational kinetics for a certain molecule is affected by the molecules in its first coordination shell. Such an analysis is useful in investigating the changes that take place in a molecule's coordination environment [70,71].

To test the ability of the GA-derived parameters in predicting the reorientational dynamics of the system, the reorientational correlation times τ_1 and τ_2 were obtained by fitting an exponential decay function in Eq. (19) to the curve obtained from the reorientational time correlation function in Eq. (18) [72].

$$C(t) = \langle P_l\left(\vec{e}(t)\cdot\vec{e}(0)\right)\rangle \tag{18}$$

$$C(t) = A\exp\left(-\frac{t}{\tau_l}\right) \tag{19}$$

where $\vec{e}(t)$ represents the unit vector along the axis of the ACN molecule, P_l is the lth-order Legendre polynomial. For the purposes of this study, the C≡N bond was chosen to define the unit vector. The calculated value can be directly compared to NMR and IR measurements studies [70,72,73]. Table 3 summarizes the reorientational correlation times obtained from the GA force field, previously developed force fields, and experimental measurements. Fig. S3 illustrates the evolution of the $C(t)$ function calculated using the GA force field.

Table 3
Calculated reorientational correlation times obtained from the GA force field, previously developed force fields, and experimental measurements.

Model	τ_1 (ps)	τ_2 (ps)
Experiment	3.28[a], 3.68[a]	1.02[a], 1.30[b]
Grabuleda et al. [64]	3.35	1.12
Vanommeslaeghe et al. [65]	4.10	1.39
Koveraga et al. [29]	2.74	0.90
Orhan et al. [66]	2.84	0.93
Kowsari et al. [35]	2.77	0.88
From GA	2.83	0.92

[a] Ref.[72]
[b] Ref.[70]

From Table 3, it can be observed that the reorientational correlation times calculated using the GA-derived parameters underestimates the experimental values. Nevertheless, the performance of the GA force field is comparable to the previously developed parameters by Koveraga et al. [29], Orhan et al. [66], and Kowsari et al. [35] On the other hand, the CHARMM force field overestimates the experimental data. Surprisingly, the reorientational times calculated using GAFF provide the best results. However, as mentioned earlier, because GAFF parameters are unable to reasonably replicate experimental physical properties, its use may be limited in conducting CMD studies.

Hence, the use of GA to optimize the parameters is an attractive strategy for future studies in force field development. From the results reported in this study, it is encouraging that the GA force field for ACN achieved excellent overall performances. Although certain physical properties, such as the density or the diffusion coefficient, are better predicted by other force fields, the GA-derived parameters show better performance for different physical properties both at room temperature and in a wide temperature range. This emphasizes the significance of the optimization methodology reported herein, where GAs can be used to optimize CMD force fields to provide useful molecular insights. The use of GA eliminates the need for manually adjusting the force field parameters as it does not require any human intervention. While the force field developed in this study (for ACN) might not be transferrable to different molecules, the use of GA offers an attractive alternative to manually optimizing the vdW parameters. In principle, this approach can be used to further optimize already available parameters, such as those present in GAFF or CHARMM, or develop new parameters for proprietary systems.

4. Conclusion

CMD simulations have attracted significant attention in recent decades as they are incredibly useful in providing insights into a wide variety of systems at the atomic level. However, the accuracy of CMD simulations is highly dependent upon the force field, i.e., the functional form for the potential energy, and the parameters used to define the intra- and intermolecular interactions in the system. To properly define any system, force field parameters that can accurately replicate experimental results are essential. Thus, the success of the CMD calculations is determined by their ability to accurately reproduce experimental properties. Although general force fields such as AMBER, OPLS, CHARMM, and GROMOS are available, their use is limited as their performance varies from one molecule to another. Because the intermolecular vdW interac-

tions are known to heavily influence the physical properties, previous work has involved intensive parameterization of the vdW parameters in order to reproduce experimental physical properties. Such methods have little to no support for simultaneous fitting of the parameters, resulting in a large number of calculations and neglect coupling effects since each parameter is fitted individually rather than a common set of calculations where all parameters are derived simultaneously. This is particularly the case for the vdW parameters, which are tightly coupled with one another. Because the hand-tuning approach involves fixing a certain parameter and adjusting the remaining parameters, the number of required calculations becomes increasingly expensive as the number of parameters increases.

Hence, we report a GA-based optimization scheme for the parameterization of intermolecular vdW terms and use ACN, a common organic solvent, to assess the GA's performance. By including both the density and the diffusion coefficient into the fitness function, we were able to optimize the vdW terms for the L-J potential to reproduce the experimental physical properties over a wide temperature range. The calculated density, diffusion coefficients, and viscosities at different temperatures with the GA-derived parameters provided better overall results in comparison with previously developed force fields. The use of FPMD simulations and experimental neutron scattering results proved incredibly useful in verifying the important interactions in ACN. In addition to the translational dynamics, our GA-derived parameters were also able to reasonably predict the reorientational dynamics as well. While previously developed L-J parameters involved manually adjusting each parameter and ignore the coupling effects between them, the GA reported herein needs no such physical intervention and can fit all the L-J terms simultaneously. Once run, the GA will automatically determine the optimum parameter set based on the properties included in the fitness function.

Future studies will extend the methodology presented in this work to other molecular systems and to more complex potential energy functions with a greater number of optimizable terms, opening up new avenues in the development of force fields that can accurately describe the physics of a system and provide useful molecular insights.

CRediT authorship contribution statement

Abdullah Bin Faheem: Investigation, Writing - original draft, Formal analysis, Software. **Jong-Yun Kim:** Writing - review & editing. **Sang-Eun Bae:** Writing - review & editing. **Kyung-Koo Lee:** Writing - review & editing, Supervision.

Declaration of Competing Interest

The authors declare that they have no known competing financial interests or personal relationships that could have appeared to influence the work reported in this paper.

Acknowledgement

This research was supported by the mid- and long-term nuclear research and development program through the National Research Foundation of Korea (NRF-2017M2A8A5014716), funded by the Korean Ministry of Science and ICT and the National Research Foundation of Korea (NRF) grant funded by the Korea government (MSIT) (NRF-2019R1A4A102980111 and NRF-2020R1I1A3066503).

Appendix A. Supplementary material

Supplementary data to this article can be found online at https://doi.org/10.1016/j.molliq.2021.116579.

References

[1] A.Y.L. Sim, P. Minary, M. Levitt, Modeling nucleic acids, Curr. Opin. Struct. Biol. 22 (2012) 273–278, https://doi.org/10.1016/j.sbi.2012.03.012.
[2] M. Karplus, J.A. McCammon, Molecular Dynamics Simulations of Biomolecules, Nat. Struct. Mol. Biol. 9 (2002) 646–652. https://doi.org/https://doi.org/10.1038/nsb0902-646.
[3] F. Vitalini, F. Noé, B.G. Keller, Molecular dynamics simulations data of the twenty encoded amino acids in different force fields, Data Br. 7 (2016) 582–590, https://doi.org/10.1016/j.dib.2016.02.086.
[4] J. Vatamanu, Z. Hu, D. Bedrov, C. Perez, Y. Gogotsi, Increasing energy storage in electrochemical capacitors with ionic liquid electrolytes and nanostructured carbon electrodes, J. Phys. Chem. Lett. 4 (2013) 2829–2837, https://doi.org/10.1021/jz401472c.
[5] R. Jorn, R. Kumar, D.P. Abraham, G.A. Voth, Atomistic modeling of the electrode-electrolyte interface in Li-ion energy storage systems: Electrolyte structuring, J. Phys. Chem. C. 117 (2013) 3747–3761, https://doi.org/10.1021/jp3102282.
[6] P.Y. Yang, S.P. Ju, H.S. Hsieh, J. Sen Lin, J.Y. Hsieh, Electrolytic molecule in-pore structure and capacitance of supercapacitors with nanoporous carbon electrodes: A coarse-grained molecular dynamics study, Comput. Mater. Sci. 166 (2019) 293–302, https://doi.org/10.1016/j.commatsci.2019.05.010.
[7] M. Takeuchi, Y. Kameda, Y. Umebayashi, S. Ogawa, T. Sonoda, Ishiguro, M. Fujita, M. Sano, Ion-ion interactions of $LiPF_6$ and $LiBF_4$ in propylene carbonate solutions, J. Mol. Liq. 148 (2009) 99–108, https://doi.org/10.1016/j.molliq.2009.07.003.
[8] S. Lee, S.S. Park, Dielectric properties of organic solvents from non-polarizable molecular dynamics simulation with electronic continuum model and density functional theory, J. Phys. Chem. B. 115 (2011) 12571–12576, https://doi.org/10.1021/jp207658m.
[9] J.K. Shah, J.F. Brennecke, E.J. Maginn, Thermodynamic properties of the ionic liquid 1-n-butyl-3-methylimidazolium hexafluorophosphate from Monte Carlo simulations, Green Chem. 4 (2002) 112–118, https://doi.org/10.1039/b110725a.
[10] C. Oostenbrink, T.A. Soares, N.F.A. Van Der Vegt, W.F. Van Gunsteren, Validation of the 53A6 GROMOS force field, Eur. Biophys. J. 34 (2005) 273–284, https://doi.org/10.1007/s00249-004-0448-6.
[11] D.S. Cerutti, W.C. Swope, J.E. Rice, D.A. Case, Ff14ipq: A self-consistent force field for condensed-phase simulations of proteins, J. Chem. Theory Comput. 10 (2014) 4515–4534, https://doi.org/10.1021/ct500643c.
[12] C.I. Bayly, K.M. Merz, D.M. Ferguson, W.D. Cornell, T. Fox, J.W. Caldwell, P.A. Kollman, P. Cieplak, I.R. Gould, D.C. Spellmeyer, A Second Generation Force Field for the Simulation of Proteins, Nucleic Acids, and Organic Molecules, J. Am. Chem. Soc. 117 (1995) 5179–5197, https://doi.org/10.1021/ja00124a002.
[13] G.A. Kaminski, R.A. Friesner, J. Tirado-Rives, W.L. Jorgensen, Evaluation and reparametrization of the OPLS-AA force field for proteins via comparison with accurate quantum chemical calculations on peptides, J. Phys. Chem. B. 105 (2001) 6474–6487, https://doi.org/10.1021/jp003919d.
[14] W.L. Jorgensen, J. Tirado-Rives, The OPLS Potential Functions for Proteins. Energy Minimizations for Crystals of Cyclic Peptides and Crambin, J. Am. Chem. Soc. 110 (1988) 1657–1666, https://doi.org/10.1021/ja00214a001.
[15] A.D. Mackerell, M. Feig, C.L. Brooks, Extending the treatment of backbone energetics in protein force fields: Limitations of gas-phase quantum mechanics in reproducing protein conformational distributions in molecular dynamics simulation, J. Comput. Chem. 25 (2004) 1400–1415, https://doi.org/10.1002/jcc.20065.
[16] A.D. MacKerell, D. Bashford, M. Bellott, R.L. Dunbrack, J.D. Evanseck, M.J. Field, S. Fischer, J. Gao, H. Guo, S. Ha, D. Joseph-McCarthy, L. Kuchnir, K. Kuczera, F.T. K. Lau, C. Mattos, S. Michnick, T. Ngo, D.T. Nguyen, B. Prodhom, W.E. Reiher, B. Roux, M. Schlenkrich, J.C. Smith, R. Stote, J. Straub, M. Watanabe, J. Wiórkiewicz-Kuczera, D. Yin, M. Karplus, All-atom empirical potential for molecular modeling and dynamics studies of proteins, J. Phys. Chem. B. 102 (1998) 3586–3616, https://doi.org/10.1021/jp973084f.
[17] J. Wang, P.A. Kollman, Automatic parameterization of force field by systematic search and genetic algorithms, J. Comput. Chem. 22 (2001) 1219–1228, https://doi.org/10.1002/jcc.1079.
[18] R.M. Betz, R.C. Walker, Paramfit: Automated optimization of force field parameters for molecular dynamics simulations, J. Comput. Chem. 36 (2015) 79–87, https://doi.org/10.1002/jcc.23775.
[19] T. Li, P.B. Balbuena, Theoretical studies of lithium perchlorate in ethylene carbonate, propylene carbonate, and their mixtures, J. Electrochem. Soc. 146 (1999) 3613–3622, https://doi.org/10.1149/1.1392523.
[20] L.B. Silva, L.C.G. Freitas, Structural and thermodynamic properties of liquid ethylene carbonate and propylene carbonate by Monte Carlo Simulations, J. Mol. Struct. THEOCHEM. 806 (2007) 23–34, https://doi.org/10.1016/j.theochem.2006.10.014.
[21] J.N.C. Lopes, A.A.H. Padua, Molecular Force Field for Ionic Liquids III: Imidazolium, Pyridinium, and Phosphonium Cations; Chloride, Bromide, and

Dicyanamide Anions, J. Phys. Chem. B. 110 (2006) 19586–19592, https://doi.org/10.1021/jp063901o.
[22] J.N.C. Lopes, A.A.H. Pádua, Molecular force field for ionic liquids composed of triflate or bistriflylimide anions, J. Phys. Chem. B. 108 (2004) 16893–16898, https://doi.org/10.1021/jp0476545.
[23] M.L.P. Price, D. Ostrovsky, W.L. Jorgensen, Gas-phase and liquid-state properties of esters, nitriles, and nitro compounds with the OPLS-AA force field, J. Comput. Chem. 22 (2001) 1340–1352, https://doi.org/10.1002/jcc.1092.
[24] M.V. Ivanov, M.R. Talipov, Q.K. Timerghazin, Genetic algorithm optimization of point charges in force field development: Challenges and insights, J. Phys. Chem. A. 119 (2015) 1422–1434, https://doi.org/10.1021/acs.jpca.5b00218.
[25] J. Wang, P. Cieplak, J. Li, Q. Cai, M.J. Hsieh, R. Luo, Y. Duan, Development of polarizable models for molecular mechanical calculations. 4. van der waals parametrization, J. Phys. Chem. B. 116 (2012) 7088–7101, https://doi.org/10.1021/jp3019759.
[26] J. Wang, T. Hou, Application of molecular dynamics simulations in molecular property prediction II: Diffusion coefficient, J. Comput. Chem. 32 (2011) 3505–3519, https://doi.org/10.1002/jcc.21939.
[27] J. Wang, T. Hou, Application of molecular dynamics simulations in molecular property prediction. 1. Density and heat of vaporization, J. Chem. Theory Comput. 7 (2011) 2151–2165, https://doi.org/10.1021/ct200142z.
[28] C. Park, M. Kanduč, R. Chudoba, A. Ronneburg, S. Risse, M. Ballauff, J. Dzubiella, Molecular simulations of electrolyte structure and dynamics in lithium–sulfur battery solvents, J. Power Sources. 373 (2018) 70–78, https://doi.org/10.1016/j.jpowsour.2017.10.081.
[29] V.A. Koverga, O.M. Korsun, O.N. Kalugin, B.A. Marekha, A. Idrissi, A new potential model for acetonitrile: Insight into the local structure organization, J. Mol. Liq. 233 (2017) 251–261, https://doi.org/10.1016/j.molliq.2017.03.025.
[30] P. Kumar, S. Yashonath, Ionic conductivity in aqueous electrolyte solutions: Insights from computer simulations, J. Mol. Liq. 277 (2019) 506–515, https://doi.org/10.1016/j.molliq.2018.12.090.
[31] V.S. Sambarivarao, O. Acevedo, Development of OPLS-AA Force Field Parameters for 68 Unique Ionic Liquids, J. Chem. Theory Comput. 5 (2009) 1038–1050, https://doi.org/10.1021/ct900009a.
[32] K. Xu, X. Ji, C. Chen, H. Wan, L. Miao, J. Jiang, Electrochemical double layer near polar reduced graphene oxide electrode: Insights from molecular dynamic study, Electrochim. Acta. 166 (2015) 142–149, https://doi.org/10.1016/j.electacta.2015.03.101.
[33] R. Wang, S. Bi, V. Presser, G. Feng, Systematic comparison of force fields for molecular dynamic simulation of Au(111)/Ionic liquid interfaces, Fluid Phase Equilib. 463 (2018) 106–113, https://doi.org/10.1016/j.fluid.2018.01.024.
[34] D. Van Der Spoel, P.J. Van Maaren, H.J.C. Berendsen, A systematic study of water models for molecular simulation : Derivation of water models optimized for use with a reaction field A systematic study of water models for molecular simulation : Derivation of water models optimized for use with a reaction fie, 10220 (2011) 10220–10230. https://doi.org/10.1063/1.476482.
[35] M.H. Kowsari, L. Tohidifar, Systematic evaluation and refinement of existing all-atom force fields for the simulation of liquid acetonitrile, J. Comput. Chem. 39 (2018) 1843–1853, https://doi.org/10.1002/jcc.25337.
[36] J. Wang, P. Cieplak, J. Li, T. Hou, R. Luo, Y. Duan, Development of polarizable models for molecular mechanical calculations I: Parameterization of atomic polarizability, J. Phys. Chem. B. 115 (2011) 3091–3099, https://doi.org/10.1021/jp112133g.
[37] P. Pahari, S. Chaturvedi, Determination of best-fit potential parameters for a reactive force field using a genetic algorithm, J. Mol. Model. 18 (2012) 1049–1061, https://doi.org/10.1007/s00894-011-1124-2.
[38] F. Leonarski, F. Trovato, V. Tozzini, A. Leś, J. Trylska, Evolutionary algorithm in the optimization of a coarse-grained force field, J. Chem. Theory Comput. 9 (2013) 4874–4889, https://doi.org/10.1021/ct4005036.
[39] B. Courcot, A.J. Bridgeman, Optimization of a Molecular Mechanics Force Field for Polyoxometalates Based on a Genetic Algorithm, J. Comput. Chem. 32 (2011) 240–247, https://doi.org/10.1002/jcc.21610.
[40] L. Chen, C.A. Morrison, T. Düren, Improving predictions of gas adsorption in metal-organic frameworks with coordinatively unsaturated metal sites: Model potentials, ab initio parameterization, and gcmc simulations, J. Phys. Chem. C. 116 (2012) 18899–18909, https://doi.org/10.1021/jp3062527.
[41] Gaussian 09, Revision D.01, M. J. Frisch, G. W. Trucks, H. B. Schlegel, G. E. Scuseria, M. A. Robb, J. R. Cheeseman, G. Scalmani, V. Barone, B. Mennucci, G. A. Petersson, H. Nakatsuji, M. Caricato, X. Li, H. P. Hratchian, A. F. Izmaylov, J. Bloino, G. Zheng, J. L. Sonnenberg, M. Hada, M. Ehara, K. Toyota, R. Fukuda, J. Hasegawa, M. Ishida, T. Nakajima, Y. Honda, O. Kitao, H. Nakai, T. Vreven, J. A. Montgomery, Jr., J. E. Peralta, F. Ogliaro, M. Bearpark, J. J. Heyd, E. Brothers, K. N. Kudin, V. N. Staroverov, T. Keith, R. Kobayashi, J. Normand, K. Raghavachari, A. Rendell, J. C. Burant, S. S. Iyengar, J. Tomasi, M. Cossi, N. Rega, J. M. Millam, M. Klene, J. E. Knox, J. B. Cross, V. Bakken, C. Adamo, J. Jaramillo, R. Gomperts, R. E. Stratmann, O. Yazyev, A. J. Austin, R. Cammi, C. Pomelli, J. W. Ochterski, R. L. Martin, K. Morokuma, V. G. Zakrzewski, G. A. Voth, P. Salvador, J. J. Dannenberg, S. Dapprich, A. D. Daniels, O. Farkas, J. B. Foresman, J. V. Ortiz, J. Cioslowski, and D. J. Fox, Gaussian, Inc., Wallingford CT, 2013.
[42] D.A. Case, T.A. Darden, T.E. Cheatham, III, C.L. Simmerling, J. Wang, R.E. Duke, R. Luo, R.C. Walker, W. Zhang, K.M. Merz, B. Roberts, S. Hayik, A. Roitberg, G. Seabra, J. Swails, A.W. Götz, I. Kolossváry, K.F.Wong, F. Paesani, J. Vanicek, R.M. Wolf, J. Liu, X. Wu, S.R. Brozell, T. Steinbrecher, H. Gohlke, Q. Cai, X. Ye, J. Wang, M.-J. Hsieh, G. Cui, D.R. Roe, D.H. Mathews, M.G. Seetin, R. Salomon-Ferrer, C. Sagui, V. Babin, T. Luchko, S. Gusarov, A. Kovalenko, and P.A. Kollman (2012), AMBER 12, University of California, San Francisco.
[43] F.Y. Dupradeau, A. Pigache, T. Zaffran, C. Savineau, R. Lelong, N. Grivel, D. Lelong, W. Rosanski, P. Cieplak, The R.E.D. tools: Advances in RESP and ESP charge derivation and force field library building, Phys. Chem. Chem. Phys. 12 (2010) 7821–7839, https://doi.org/10.1039/c0cp00111b.
[44] A.M. Nikitin, A.P. Lyubartsev, New Six-site Acetonitrile Model for Simulations of Liquid Acetonitrile and its Aqueous Mixtures, J. Comput. Chem. 28 (2007) 2020–2026, https://doi.org/10.1002/jcc.20721.
[45] H.V.T. Nguyen, K. Kwak, K.K. Lee, 1,1-Dimethylpyrrolidinium tetrafluoroborate as novel salt for high-voltage electric double-layer capacitors, Electrochim. Acta. 299 (2019) 98–106, https://doi.org/10.1016/j.electacta.2018.12.155.
[46] P. Alston Steiner, W. Gordy, Precision measurement of dipole moments and other spectral constants of normal and deuterated methyl fluoride and methyl cyanide, J. Mol. Spectrosc. 21 (1966) 291–301, https://doi.org/10.1016/0022-2852(66)90152-4.
[47] L. Angibaud, L. Briquet, P. Philipp, T. Wirtz, J. Kieffer, Parameter optimization in molecular dynamics simulations using a genetic algorithm, Nucl. Instruments Methods Phys. Res. Sect. B Beam Interact. with Mater. Atoms. 269 (2011) 1559–1563, https://doi.org/10.1016/j.nimb.2010.11.024.
[48] J.M.C. Marques, F.V. Prudente, F.B. Pereira, M.M. Almeida, A.M. Maniero, C.E. Fellows, A new genetic algorithm to be used in the direct fit of potential energy curves to ab initio and spectroscopic data, J. Phys. B At. Mol. Opt. Phys. 41 (2008), https://doi.org/10.1088/0953-4075/41/8/085103.
[49] L. Martínez, R. Andrade, E.G. Birgin, J.M. Martínez, PACKMOL: A package for building initial configurations for molecular dynamics simulations, J. Comput. Chem. 30 (2009) 2157–2164, https://doi.org/10.1002/jcc.21224.
[50] A. Mondal, J.M. Young, T.A. Barckholtz, G. Kiss, L. Koziol, A.Z. Panagiotopoulos, Genetic Algorithm Driven Force Field Parameterization for Molten Alkali-Metal Carbonate and Hydroxide Salts, J. Chem. Theory Comput. (2020), https://doi.org/10.1021/acs.jctc.0c00285.
[51] K. Hickey, W.E. Waghorne, Viscosities and volumes of dilute solutions of formamide in water + acetonitrile and for formamide and N, N-dimethylformamide in methanol + acetonitrile mixed solvents: Viscosity B-Coefficients, activation free energies for viscous flow, and partial molar, J. Chem. Eng. Data. 46 (2001) 851–857, https://doi.org/10.1021/je0003647.
[52] E. Hawlicka, R. Grabowski, Solvation of Ions in Acetonitrile-Methanol Solutions of Sodium Iodide, Berichte Der Bunsengesellschaft Für Phys. Chemie. 94 (1990) 486–489, https://doi.org/10.1002/bbpc.19900940413.
[53] P. Sharma, A. Wadhwa, K. Komal, Analysis of Selection Schemes for Solving an Optimization Problem in Genetic Algorithm, Int. J. Comput. Appl. 93 (2014) 1–3, https://doi.org/10.5120/16256-5714.
[54] K. Deb, A. Pratap, S. Agarwal, T. Meyarivan, A fast and elitist multiobjective genetic algorithm: NSGA-II, IEEE Trans. Evol. Comput. 6 (2002) 182–197, https://doi.org/10.1109/4235.996017.
[55] A. Konak, D.W. Coit, A.E. Smith, Multi-objective optimization using genetic algorithms: A tutorial, Reliab. Eng. Syst. Saf. 91 (2006) 992–1007, https://doi.org/10.1016/j.ress.2005.11.018.
[56] S. Plimpton, Fast parallel algorithms for short-range molecular dynamics, J. Comput. Phys. 117 (1995) 1–19, https://doi.org/10.1006/jcph.1995.1039.
[57] S. Nosé, A unified formulation of the constant temperature molecular dynamics methods, J. Chem. Phys. 81 (1984) 511–519, https://doi.org/10.1063/1.447334.
[58] W.G. Hoover, Canonical dynamics: Equilibrium phase-space distributions, Phys. Rev. A. 31 (1985) 1695, https://doi.org/10.1103/PhysRevA.31.1695.
[59] J. Vandevondele, M. Krack, F. Mohamed, M. Parrinello, T. Chassaing, J. Hutter, Quickstep: Fast and accurate density functional calculations using a mixed Gaussian and plane waves approach, Comput. Phys. Commun. 167 (2005) 103–128, https://doi.org/10.1016/j.cpc.2004.12.014.
[60] S. Grimme, J. Antony, S. Ehrlich, H. Krieg, A consistent and accurate ab initio parametrization of density functional dispersion correction (DFT-D) for the 94 elements H-Pu, J. Chem. Phys. 132 (2010), https://doi.org/10.1063/1.3382344.
[61] E.M. Kirova, G.E. Norman, Viscosity calculations at molecular dynamics simulations, J. Phys. Conf. Ser. 653 (2015), https://doi.org/10.1088/1742-6596/653/1/012106.
[62] J. Ma, Z. Zhang, Y. Xiang, F. Cao, H. Sun, On the prediction of transport properties of ionic liquid using 1-n-butylmethylpyridinium tetrafluoroborate as an example, Mol. Simul. 43 (2017) 1502–1512, https://doi.org/10.1080/08927022.2017.1321760.
[63] P.E. Smith, W.F. van Gunsteren, The viscosity of SPC and SPC/E water at 277 and 300 K, Chem. Phys. Lett. 215 (1993) 315–318, https://doi.org/10.1016/0009-2614(93)85720-9.
[64] X. Grabuleda, C. Jaime, P.A. Kollman, Molecular Dynamics Simulation Studies of Liquid Acetonitrile: New Six-Site Model, J. Comput. Chem. 21 (2000) 901–908, https://doi.org/10.1002/1096-987X(20000730)21:10<901::AID-JCC7>3.0.CO;2-F.
[65] K. Vanommeslaeghe, E. Hatcher, C. Acharya, S. Kundu, S. Zhong, J. Shim, E. Darian, O. Guvench, P. Lopes, I. Vorobyov, A.D. MacKerell, CHARMM General Force Field: A Force Field for Drug-Like Molecules Compatible with the CHARMM All-Atom Additive Biological Force Fields, J. Comput. Chem. 31 (2010) 671–690, https://doi.org/10.1002/jcc.21367.
[66] M. Orhan, Dielectric and transport properties of acetonitrile at varying temperatures: A molecular dynamics study, Bull. Korean Chem. Soc. 35 (2014) 1469–1478, https://doi.org/10.5012/bkcs.2014.35.5.1469.

[67] R.L. Hurle, L.A. Woolf, Self-diffusion in liquid acetonitrile under pressure, J. Chem. Soc. Faraday Trans. 1 Phys. Chem. Condens. Phases. 78 (1982) 2233–2238. https://doi.org/10.1039/F19827802233.

[68] J.H. Dymond, M.A. Awan, N.F. Glen, J.D. Isdale, Transport properties of nonelectrolyte mixtures. IX. Viscosity coefficients for acetonitrile and for three mixtures of toluene+acetonitrile from 25 to 100°c at pressures up to 500 MPa, Int. J. Thermophys. 12 (1991) 433–447, https://doi.org/10.1007/BF00502360.

[69] E.K. Humphreys, P.K. Allan, R.J.L. Welbourn, T.G.A. Youngs, A.K. Soper, C.P. Grey, S.M. Clarke, A Neutron Diffraction Study of the Electrochemical Double Layer Capacitor Electrolyte Tetrapropylammonium Bromide in Acetonitrile, J. Phys. Chem. B. 119 (2015) 15320–15333, https://doi.org/10.1021/acs.jpcb.5b08248.

[70] K. Yuan, H. Bian, Y. Shen, B. Jiang, J. Li, Y. Zhang, H. Chen, J. Zheng, Coordination number of Li^+ in nonaqueous electrolyte solutions determined by molecular rotational measurements, J. Phys. Chem. B. 118 (2014) 3689–3695, https://doi.org/10.1021/jp500877u.

[71] J. Boisson, G. Stirnemann, D. Laage, J.T. Hynes, Water reorientation dynamics in the first hydration shells of F^- and I^-, Phys. Chem. Chem. Phys. 13 (2011) 19895–19901, https://doi.org/10.1039/c1cp21834d.

[72] P.J. Gee, W.F. Van Gunsteren, Acetonitrile revisited: A molecular dynamics study of the liquid phase, Mol. Phys. 104 (2006) 477–483, https://doi.org/10.1080/00268970500473450.

[73] A. Sugitani, S. Ikawa, S. Konaka, Effect of temperature on the infrared band shapes and reorientational and vibrational relaxation of liquid acetonitrile, Chem. Phys. 142 (1990) 423–430, https://doi.org/10.1016/0301-0104(90)80037-X.